

Article

Numerical Investigation on Higher-Order Harmonic Waves Induced by a Submerged Inclined Plate

Zhimin Zhou ¹, Yawei Sun ^{2,*} , Lifen Chen ^{2,*}, Dezhi Ning ²  and Sulisz Wojciech ³

¹ Science and Technology on Underwater Test and Control Laboratory, The 760th Research Institute of China Shipbuilding Industry Corporation, Dalian 116013, China

² The State Key Laboratory of Coastal and Offshore Engineering, Dalian University of Technology, Dalian 116024, China

³ Institute of Hydro-Engineering, Polish Academy of Science, Palace of Culture and Science, Plac Defilad 1, Skrytka Pocztoowa 24, 00-901 Warszawa, Poland

* Correspondence: yaweisun@mail.dlut.edu.cn (Y.S.); lifen_chen@dlut.edu.cn (L.C.)

Abstract: In this paper, a two-dimensional time-domain numerical flume has been established to model and investigate nonlinear interactions between nonlinear surface waves and a submerged inclined thin plate. The model solves the Laplace equation and the fully nonlinear free surface boundary conditions within the framework of potential flow theory based on the high-order boundary element method. The mixed Euler–Lagrangian method is applied to update the water surface at each time step, and the fourth-order Runge–Kutta method for time stepping. A so-called four-point method was employed to separate the second-order harmonic free and bounded wave that has the same wave frequency but different wave celerity in front of and behind the submerged plate. It is found that the amplitude of the second-order harmonic free wave increases with the inclination angle of the submerged plate, and the level/amount of the increase is larger for a larger wave steepness. In addition, the amplitudes of both the second-order reflected and transmitted waves are found to increase with the wave steepness, and their empirical relationships are derived for potential use in practical engineering.

Keywords: submerged inclined plate; fully nonlinear numerical wave flume; higher-order harmonic waves; high-order boundary element method



Citation: Zhou, Z.; Sun, Y.; Chen, L.; Ning, D.; Wojciech, S. Numerical Investigation on Higher-Order Harmonic Waves Induced by a Submerged Inclined Plate. *J. Mar. Sci. Eng.* **2022**, *10*, 1115. <https://doi.org/10.3390/jmse10081115>

Academic Editor: Dong-Sheng Jeng

Received: 7 July 2022

Accepted: 11 August 2022

Published: 13 August 2022

Publisher's Note: MDPI stays neutral with regard to jurisdictional claims in published maps and institutional affiliations.



Copyright: © 2022 by the authors. Licensee MDPI, Basel, Switzerland. This article is an open access article distributed under the terms and conditions of the Creative Commons Attribution (CC BY) license (<https://creativecommons.org/licenses/by/4.0/>).

1. Introduction

Breakwater in various forms is widely employed in coastal engineering for protecting structures and/or the coastal line behind. Traditional bottom-mounted breakwater generally requires a solid foundation and consumes a large number of materials, resulting in high construction costs. In addition, the water circulation, i.e., the movement and exchange of water, between the open sea and the coastal area is interrupted as the main body of the breakwater extends from the sea bed and pierces the sea surface. This may lead to water pollution and destroys the sediment balance (i.e., coastal erosion) of the protected area. The ecological environment of the local waters may also be altered; the change in the seawater salinity and temperature may be introduced by the sewage disposal [1–3].

Compared with the traditional impermeable bottom-mounted breakwater mentioned above, the breakwater consisting of a submerged plate has the advantages of having lower requirements in terms of foundation condition and enhanced water exchange (the water flows freely underneath) [4]. The design consisting of a truncated structure, i.e., a structure arranged on the water surface, is also a good alternative. Such a design works better for attenuating the water height but may have an adverse effect on the landscape. The former, which works to reduce the incoming wave energy to an acceptable level and is landscape-friendly, is the focus of this work. When working as a breakwater, in order to achieve a relatively stable berthing condition on the leeward side, such as in harbor

areas, it is necessary to understand better the mechanism of the interaction between the submerged plate and surface waves (c.f. reflection and transmission of the breakwater). It is also worth noting that the potential of using the submerged (artificial) reefs as coastal solutions for shoreline control, etc., has also attracted increasing attention within the field [5]. The reef may be composed of geosynthetic bags filled with loose materials, i.e., a sand-filled geosystem.

In addition, a submerged plate is also widely used as one of the key components of a wave energy conversion (WEC) device for wave energy capturing [6–8]. The submerged plate moves with the incoming waves, converting the wave energy to kinetic energy and then electricity. There are also WEC devices integrated with breakwater, which have the functions of both wave dissipation and power generation [9–11]. For example, references [12,13] proposed a WEC concept consisting of six hinged submerged plates, and the associated characteristics in terms of reflection/transmission and power extraction are detailed. The former is essential for the function of breakwater, and understanding the wave behaviors when it propagates toward and over the plate is an essential step to improving the conversion efficiency of the device.

Generally, a regular wave of sinusoidal or cosine shape experiences a strong deformation when it propagates toward and over a submerged structure due to the shallow-water effect, leading to the generation of higher-order harmonic waves. These higher harmonics have wave frequencies that are close to integer multiples of the fundamental frequency and initially propagate with the fundamental wave component, i.e., the so-called higher-order bounded waves. Partial wave energy (consisting of the incident fundamental and the generated higher-order harmonic waves) is then reflected, and the rest continues to travel over the submerged structure, and these (reflected and transmitted) waves experience another depth transition from shallow to deep. During this process, the aforementioned higher-order bounded waves may be released as free waves, i.e., the corresponding wave frequency and wave number satisfy the dispersion relation. The word ‘free’ indicates that these higher harmonics now propagate freely with their own wave celerity rather than bounded with the fundamental wave. The local wave field is thus very complex and may have adverse effects on the capacities of the breakwater and the wave energy converter that are composed of a submerged plate. Therefore, it is of great significance to investigate the higher-order harmonic waves induced by a submerged inclined plate, which forms the focus of this study.

Extensive research on wave propagation over a submerged structure has been carried out in past decades. An analytical formula was derived in [14] for calculating wave reflection from and transmission over an upright submerged plate in deep waters. The latter is an important factor for evaluating the performance or efficiency of a breakwater. Later, the problem of wave diffraction around a semi-infinite submerged plane barrier placed in finite-depth water was studied in [15], and the problem was solved by employing the Wiener–Hopf Fourier transform method. These (the calculation of wave diffraction as well as reflection and transmission coefficients) have been extended in [16] to the cases of infinite water depth and been further extended in [17] to the submerged plate of finite length. The wave reflection from submerged plates in shallow waters is the main subject in [18]. The occurrence conditions for total/full- and zero-reflection are identified theoretically. The results show that the reflection coefficient increases with the decrease in the ratio of submergence (the water depth above the submerged plate) to the water depth (measured away from the submerged plate) and the ratio of the water depth to the wavelength. In addition, it is found to increase firstly with the ratio between the plate width and the wavelength to its maximum value and then decrease to zero with a further increase. An analytical model for investigating the interaction between an oblique wave and a horizontal submerged flexible porous plate was developed in [19]. The results indicate that the attack angle between the wave and the plate and the mooring stiffness are the two important factors that affect the wave energy absorption of the system significantly.

It is noted that the studies mentioned above solve the problems theoretically/analytically and hence are mainly within the framework of linear wave theory. For more practical application, nonlinear wave diffraction by a rectangular submerged plate or a horizontal cylinder in deep waters was studied experimentally and numerically in [20], although the waves considered were still of low amplitude. The models solved the Boussinesq equation in shallow waters and the Laplace equation (within the framework of linear potential flow theory) in deep waters. It is found that the generation of higher-order harmonic waves on the leeward side becomes stronger when the incident wave amplitude is increased. The propagation of regular waves toward and over a submerged horizontal plate in a current flow was simulated in [21]. The influence of the current on the second-order free wave was investigated, and it was found that the beat length (periodicity in space) was an important parameter for analyzing the second-order free wave; the longer the beat length was, the stronger the energy exchange between the fundamental and the higher-order harmonic waves was. In [22], a two-dimensional fully nonlinear numerical wave flume based on the higher-order boundary element method (HOBEM) in the time domain to investigate nonlinear wave-current-submerged plate interactions was established. A so-called two-point method [20] was employed to extract the higher-order bounded and free harmonic waves upstream and downstream of the structure. It is found that the second-order free wave is more sensitive to the introduction of the current when compared to the linear component, and the adverse current is more influential than the following counterpart. The adverse and following currents propagate in opposite and the same directions as the incoming wave, respectively. It is worth noting that the submerged plates involved here are vertical and/or horizontal, and the effect of inclined angle is not considered.

The study of the linear interaction between a wave and a fixed inclined plate indicates that the submerged breakwater composed of an inclined plate is desirable [23]. The peak reflection coefficient is found to increase from 10% to 40% when the inclined angle increases from 30° to 60° (the angle between the horizontal line and the plate centerline). In [24], the problem of two submerged inclined plates placed side-by-side was considered, and better performance in terms of wave reflection was found when compared to the case of a single inclined plate. The effect of the inclination direction (i.e., inclined upstream or downstream) was investigated by using the physical experiments in combination with numerical simulations in [25]. In [26], the authors found that a thin plate with an inclination angle of 60° works well across all the wave parameters considered, and a maximum reduction of 40% in the wave height was found. It is then clear that a systematic investigation of the induced higher-order harmonic waves is still required.

In this paper, the nonlinear interaction between a nonlinear regular wave and a submerged plate of various inclination angles is studied numerically based on the HOBEM within the framework of potential flow theory. The numerical model is verified firstly by comparing with the published experimental and numerical results. The generation of higher harmonic waves and its effect on the hydrodynamic performance of the system are then investigated in detail. The relationships between the generated 2nd-order free wave and the inclination angle as well as the incoming wave amplitude are explored.

2. Numerical Methods

2.1. Fully Nonlinear Numerical Wave Tank

Figure 1 shows the schematic diagram of the considered problem in two-dimension. The applied Cartesian coordinate system is also shown: the x -axis is positive when pointing to the right and its origin is at the left end of the tank, and the y -axis is positive upward with $y = 0$ at the mean water surface, and d is the water depth. In theory, the fully nonlinear numerical wave tank (NWT) established in this work can simulate nonlinear wave evolution in the water of an arbitrary depth [27], although only shallow and intermediate water depths are considered in this work. The submerged inclined plate is characterized by the inclination angle α and the submergence d' (the vertical distance between the plate center and the mean water surface). L and w are the length and the thickness of the plate,

respectively. These two were kept constant in this work, and the submerged inclined plate was placed at the mid-aft of the NWT.

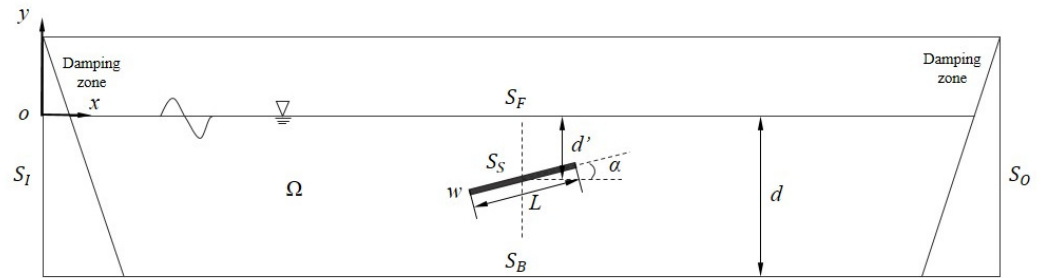


Figure 1. Sketch of the 2-D numerical wave tank (front view).

Ω denotes the computation domain, which is bounded by the incident boundary S_I , the free surface S_F , the outflow boundary S_O , and the solid boundaries consisting of the impermeable submerged plate S_S and the seabed S_B .

For the NWT established within the framework of the potential flow theory, the fluid is assumed to be inviscid and incompressible, and the fluid motion irrotational. Thus, the fluid motion can be described by the velocity potential $\Phi(x, y, t)$, which satisfies the Laplace equation (see Equation (1)) in the computational domain Ω shown in Figure 1.

Here, the dynamics of the instantaneous water surface S_F are described by the fully nonlinear kinematic and dynamic boundary conditions. The seabed (S_B), the left incident boundary (S_I) and the right outflow boundaries (S_O) of the NWT as well as the submerged structure (S_S) are considered to be impermeable, i.e., the normal velocity at these boundaries is set to zero.

That is, the considered boundary value problem can be mathematically described as,

$$\begin{cases} \nabla^2 \Phi = 0, & \text{in } \Omega \\ \frac{\partial \eta}{\partial t} = \frac{\partial \Phi}{\partial y} - v_1(x)(\eta - \eta_0) - v_2(x)\eta, & \text{on } S_F \\ \frac{\partial \Phi}{\partial t} = -g\eta + \frac{1}{2}|\nabla \Phi|^2 - v_1(x)(\Phi - \Phi_0) - v_2(x)\Phi, & \text{on } S_F \\ \frac{\partial \Phi}{\partial t} = \frac{\partial \Phi_I}{\partial n} = -\frac{\partial \Phi_I}{\partial x}, & \text{on } S_I \\ \frac{\partial \Phi}{\partial n} = 0, & \text{on } S_B, S_S, S_O \end{cases} \quad (1)$$

where the gradient operator $\nabla = \left(\frac{\partial}{\partial x}, \frac{\partial}{\partial y}\right)$, g and η are the acceleration due to gravity and the free surface elevation, respectively. t and x are the time and the horizontal distance away from the inlet boundary respectively. η_0 and Φ_0 are the undisturbed free surface elevation and the velocity potential calculated by the second-order analytical solution derived in [28]. Furthermore, Φ_I is the incident velocity potential.

In this work, the method of numerical beach is applied for absorbing reflected waves from the domain, and hence additional damping terms involving the damping coefficients $v_1(x)$ and $v_2(x)$ are introduced

$$v_{1(2)}(x) = \begin{cases} \alpha_d \omega \left(\frac{x-x_{1(2)}}{L_b}\right)^2 & (x < x_1 \text{ or } x > x_2) \\ 0 & \text{others} \end{cases} \quad (2)$$

where ω is the wave angular frequency, x_1 and x_2 are the starting positions of the damping zones at both ends of the NWT, respectively. α_d denotes the damping coefficient, which is selected as $\alpha_d = 1.0$, in this work, L_b is the length of the damping zone, which is empirically selected as $L_b = 2\lambda$ [21] in which λ is the wavelength of the incident wave propagating from left to right.

The second-order Stokes theoretical solution of incident velocity potential on the incident boundary S_I is given by

$$\Phi_I = \frac{ga}{\omega} \frac{\cosh k(y+d)}{\cosh kd} \sin(kx - \omega t) + \frac{3}{8} ka^2 \omega \frac{\cosh 2k(y+d)}{\sinh^4 kd} \sin 2(kx - \omega t) \quad (3)$$

where a is the wave amplitude and the wave number k is determined by the dispersion relation,

$$\omega^2 = gk \tanh kd \quad (4)$$

The Equation (4) is normally solved numerically by using the iterative method, while the high-precision fitting formula is also widely used to speed up the calculation [29],

$$(kd)^2 = U^2 + \frac{U}{1 + \sum_{n=1}^6 V_n U^n} \quad (5)$$

where $U = \omega^2 d/g$, $V_1 = 0.66667$, $V_2 = 0.35556$, $V_3 = 0.16084$, $V_4 = 0.06321$, $V_5 = 0.02175$, and $V_6 = 0.00654$. Noted that the wave period T or the wave frequency ω is considered to be known here. The dispersion relation indicates that the wave with a different wave period travels with a different speed and also dependent on the water depth.

It is worth noting that for a wave propagating in shallow water (i.e., $\frac{d}{\lambda} \leq \frac{1}{20}$), Equation (4) is simplified to be $\omega^2 = gk(kd)$ and the wave speed is expressed as $c = \frac{\omega}{k} = \sqrt{gd}$. This indicates that the wave dose not disperse with the wave period/frequency. In deep waters (i.e., $\frac{d}{\lambda} \geq \frac{1}{2}$), the Equation (4) is implied as $\omega^2 = gk$, which indicates that the wave speed is independent with the water depth only here.

By applying the second Green's theorem, the above boundary value problem can be transformed into the boundary integral equation:

$$\alpha(p)\Phi(p) = \int_S \left(\Phi(q) \frac{\partial G(q,p)}{\partial n} - G(q,p) \frac{\partial \Phi(q)}{\partial n} \right) dS, \quad p \in S \quad (6)$$

where $p = (x_0, y_0)$ and $q = (x, y)$ are the source points and the field points, respectively. $\alpha(p)$ is the solid angle coefficient associated with the surface geometry of the source point p , and $S = S_I + S_F + S_O + S_S$. It is worth noting that the bottom of the NWT (S_B) is excluded from the integral by adding the mirror images of the Rankine sources at the seabed. $G(q, p)$ is the simple Green function,

$$G(q, p) = \frac{1}{2\pi} (\ln r_1 + \ln r_2) \quad (7)$$

$$r_1 = \sqrt{(x - x_0)^2 + (y - y_0)^2} \quad (8)$$

$$r_2 = \sqrt{(x - x_0)^2 + (y - y_0 + 2d)^2} \quad (9)$$

where r_1 is the distance between the field point and the source point, and r_2 is the distance between the field point and its mirror image with respect to the seabed.

The boundary integral equation, Equation (6), is solved by the higher-order boundary element method (HOBEM), in which the boundary S is discretized into a set of three-node elements. The variables of interest, including the geometric coordinates, the velocity potential, and their normal derivatives, at an arbitrary point within an element, can then be represented by the nodal values via the quadratic shape function. A set of linear algebraic equations is obtained by assembling the equations for each node on the entire boundary S at each time step [30]. The fourth-order Runge–Kutta (RK4) scheme [31] is used to advance the free surface from the initial quiet state to the time instant of interest. More details are referred to in [21].

2.2. The Four-Point Method for Extracting Higher-Order Bounded and Free Harmonic Waves

The method for separating incident and reflected waves was firstly proposed in [32], in which the total signals measured by two adjacent wave gauges are used, i.e., the so-called two-point method. This method assumes that the higher-order harmonic waves travel with the linear components. An extended two-point method is then proposed in [20] for separating the high-order free and bounded harmonic waves before and after a submerged structure. The least square method for separating the incident and reflected waves using the data of three points was proposed in [33], i.e., the so-called three-point method. Subsequently, a nonlinear reflection analysis method to separate free and bounded waves up to second-order was developed in [34]. For a more accurate and clearer separation, using measurements at four or more points was suggested in [20,35]. The performance of the two-point, three-point and four-point separation methods mentioned above has been discussed and compared in detail in [36]. In general, the four-point method is considered to work better; hence, it is also employed in this work.

The free surface elevation at a point of x away from the wave paddle and on the weather side can be expressed as:

$$\begin{aligned} \eta(x, t) = & a_I^{(1)} \cos(k^{(1)}x - \omega t + \varphi_I^{(1)}) + a_R^{(1)} \cos(k^{(1)}x - \omega t + \varphi_R^{(1)}) + \sum_{n \geq 2}^{\infty} a_{IB}^{(n)} \cos[n(k^{(1)}x - \omega t) + \varphi_{IB}^{(n)}] \\ & + \sum_{n \geq 2}^{\infty} a_{RB}^{(n)} \cos[n(k^{(1)}x - \omega t) + \varphi_{RB}^{(n)}] + \sum_{n \geq 2}^{\infty} a_{IF}^{(n)} \cos[(k^{(1)}x - n\omega t) + \varphi_{IF}^{(n)}] \\ & + \sum_{n \geq 2}^{\infty} a_{RF}^{(n)} \cos[(k^{(1)}x - n\omega t) + \varphi_{RF}^{(n)}] \end{aligned} \tag{10}$$

where the subscripts IB, IF, RB and RF represent the incident bounded and free wave, the reflected bounded and free wave, respectively.

Here we introduce the Fourier transform:

$$\hat{\eta}^{(n)}(x) = \frac{\omega}{2\pi} \int_0^{\frac{2\pi}{\omega}} \eta(x, t) \exp(-i\omega t) dt \quad n = 1, 2, 3 \dots \tag{11}$$

Substitute Equation (10) into Equation (11) we obtained ($n \geq 2$):

$$\hat{\eta}^{(n)}(x) = C_{IB}^{(n)} X_{IB}^{(n)} + C_{RB}^{(n)} X_{RB}^{(n)} + C_{IF}^{(n)} X_{IF}^{(n)} + C_{RF}^{(n)} X_{RF}^{(n)} \tag{12}$$

$$\begin{aligned} X_{IB}^{(n)} &= a_{IB}^{(n)} \exp[-i(nk^{(1)}x + \varphi_{IB}^{(n)})]; X_{RB}^{(n)} = a_{RB}^{(n)} \exp[i(nk^{(1)}x + \varphi_{RB}^{(n)})] \\ X_{IF}^{(n)} &= a_{IF}^{(n)} \exp[-i(nk^{(n)}x + \varphi_{IF}^{(n)})]; X_{RF}^{(n)} = a_{RF}^{(n)} \exp[i(nk^{(n)}x + \varphi_{RF}^{(n)})] \end{aligned} \tag{13}$$

$$\begin{aligned} C_{IB}^{(n)} &= \frac{\exp[-i(nk^{(1)}\Delta x_m)]}{2}; C_{RB}^{(n)} = \frac{\exp[i(nk^{(1)}\Delta x_m)]}{2} \\ C_{IF}^{(n)} &= \frac{\exp[-i(nk^{(n)}\Delta x_m)]}{2}; C_{RF}^{(n)} = \frac{\exp[i(nk^{(n)}\Delta x_m)]}{2} \end{aligned} \tag{14}$$

where Δx_m represents the distance between the m point and the first point.

If the measurements at four points on the weather side are considered, the equation for free and bounded waves are obtained:

$$\begin{bmatrix} C_{1IB}^{(n)} & C_{1RB}^{(n)} & C_{1IF}^{(n)} & C_{1RF}^{(n)} \\ C_{2IB}^{(n)} & C_{2RB}^{(n)} & C_{2IF}^{(n)} & C_{2RF}^{(n)} \\ C_{3IB}^{(n)} & C_{3RB}^{(n)} & C_{3IF}^{(n)} & C_{3RF}^{(n)} \\ C_{4IB}^{(n)} & C_{4RB}^{(n)} & C_{4IF}^{(n)} & C_{4RF}^{(n)} \end{bmatrix} \begin{bmatrix} X_{IB}^{(n)} \\ X_{RB}^{(n)} \\ X_{IF}^{(n)} \\ X_{RF}^{(n)} \end{bmatrix} = \begin{bmatrix} \hat{\eta}^{(n)}(x_1) \\ \hat{\eta}^{(n)}(x_2) \\ \hat{\eta}^{(n)}(x_3) \\ \hat{\eta}^{(n)}(x_4) \end{bmatrix} \tag{15}$$

After solving the matrix Equation (15), the amplitude of the free and bounded wave can be obtained:

$$\begin{aligned} a_{IB}^{(n)} &= \text{abs}(X_{IB}^{(n)}); a_{RB}^{(n)} = \text{abs}(X_{RB}^{(n)}) \\ a_{IF}^{(n)} &= \text{abs}(X_{IF}^{(n)}); a_{RF}^{(n)} = \text{abs}(X_{RF}^{(n)}) \end{aligned} \tag{16}$$

In order to prevent singularity when solving the matrix Equation (15), the basic condition is given [35]:

$$\Delta x_2 \neq m \frac{\lambda}{2}, \Delta x_3 \neq s \Delta x_2, \Delta x_4 \neq r \Delta x_2, \Delta x_3 \neq t \Delta x_4 \tag{17}$$

where m, s, r and t are all positive integers.

For transmitted waves, the subscripts I, IB and IF are replaced by T, TB and TF to represent the transmitted fundamental wave, the transmitted bounded and free waves. The high-order bounded and free wave amplitude on the leeward side can be calculated by the same method mentioned above.

The reflection and transmission coefficients of the fundamental wave can then be calculated:

$$k_r = \frac{a_R^{(1)}}{a_I^{(1)}}; k_t = \frac{a_T^{(1)}}{a_I^{(1)}} \tag{18}$$

3. Numerical Results and Discussion

In this section, the established model is firstly verified by comparing the experimental measurements carried out at Dalian University of Technology, China and the numerical results published in [23]. The verified NWT is then used to study the interaction mechanism between waves and a submerged inclined plate. The behaviors of the higher-order free waves generated above the submerged inclined plate are discussed.

3.1. Model Validation

3.1.1. Experiment Setup

A physical experiment, as shown in Figure 2, was carried out in a wave flume ($22 \times 0.5 \times 0.6$) at the State Key Laboratory of Coastal and Offshore Engineering, Dalian University of Technology, Dalian, China. A hydraulic piston-type wave maker is installed at one end for generating incident waves, and there is a sloping beach at the opposite end to diminish wave reflection. The water depth was $d = 0.4$ m, and the acrylic submerged plate with a thickness of $w = 10$ mm and a length of $L = 0.4$ m (see Figure 3), placed 9.36 m away from the wave maker.

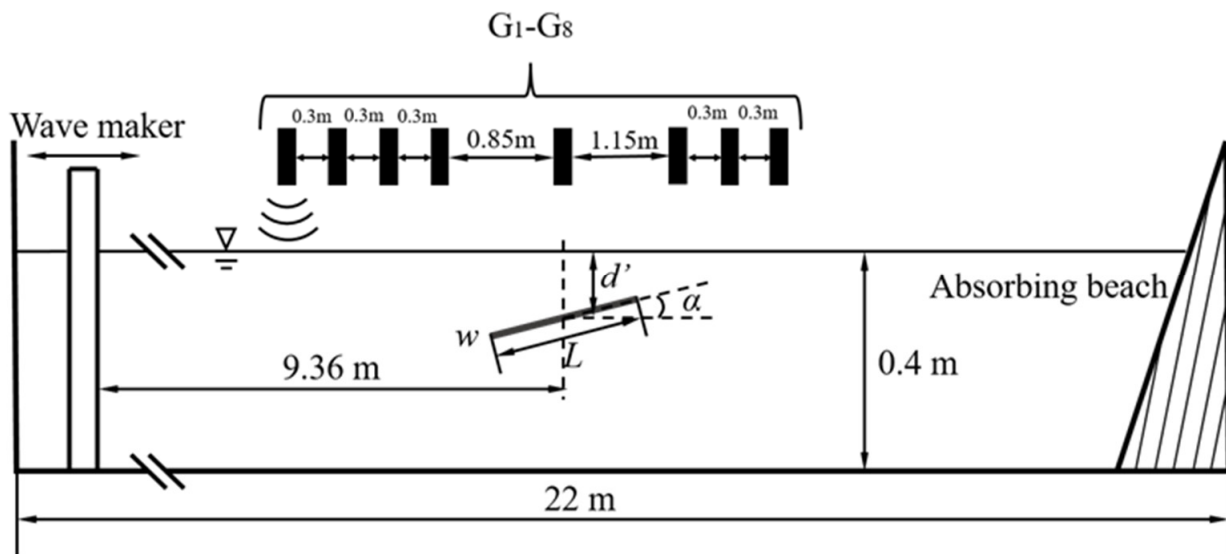


Figure 2. Experimental layout: a side view showing the submerged plate and the wave gauges.

A set of ultrasonic wave gauges, G_1 – G_4 , were placed on the weather side of the plate with a constant spacing of 0.3 m for resolving the reflected waves. G_5 was placed directly above the submerged plate, and the distance between G_4 and G_5 was 0.85 m. Three wave

gauges, G_6 – G_8 , were placed on the leeward side of the plate to resolve the transmitted waves. The spacing was also 0.3 m, and the distance between G_5 and G_6 was 1.15 m. It should be noted that the wave gauges were numbered sequentially from left to right in Figure 2, i.e., the leftmost wave gauge was labeled G_1 , and the rightmost was G_8 . The wave gauges and its acquisition system are shown in Figure 4.



Figure 3. The inclined submerged plate in the experiment which is highlighted by the red line.



Figure 4. Wave gauges (top) and its acquisition system (bottom).

It should be noted that only two typical cases in the experiment are selected here to verify the numerical model.

3.1.2. Numerical Model for Nonlinear Wave Evolution

A numerical flume without a structure in place is firstly established with a tank length of $TL = 14\lambda$. Simulations with three different time steps and three different mesh sizes are

carried out to ensure that the results are time-step and mesh-independent. The example case considered/shown here has a wave period of $T = 1.06$ s and the dimensionless parameter of $a/d = 0.05$; recall that λ is the wavelength, a the incident wave amplitude and d the water depth.

Figure 5 shows the time series of the free surface elevation measured at $x = 8\lambda$ for the set of time-steps and mesh considered. It can be seen that the results are convergent using the medium size of the time step and mesh, and hence the time step of $\Delta t = T/40$, and the mesh size of $\Delta x = \lambda/35$ are used hereafter.

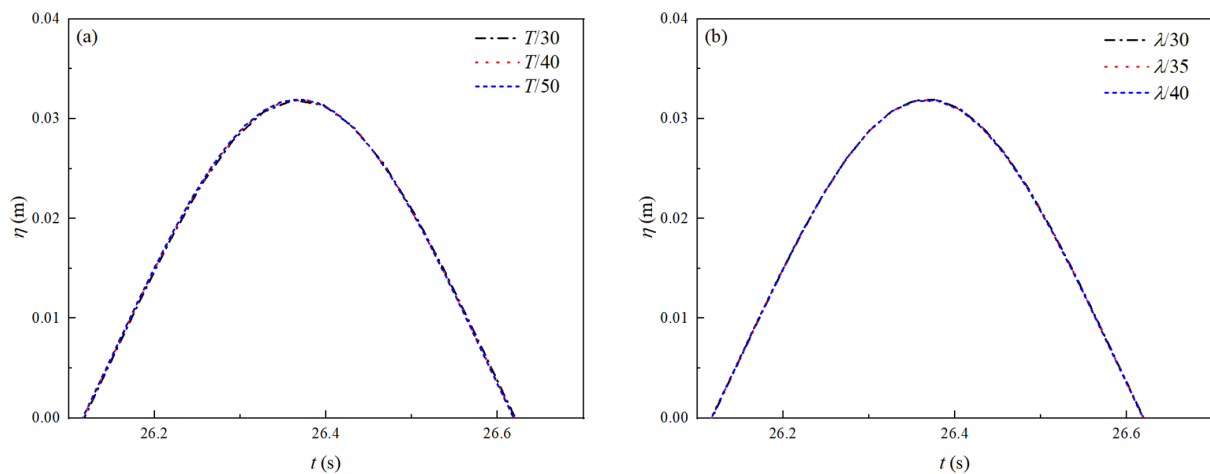


Figure 5. The time series of the free surface elevation at $x = 8\lambda$ calculated using (a) three different time steps; and (b) three different mesh sizes.

It should be noted that the mesh size used for the simulations shown in Figure 5a is $\Delta x = \lambda/35$, and the time step used in Figure 5b is $\Delta t = T/40$. The vertical mesh size at the incident and outflow boundaries is $\Delta y = d/20$ [21,37].

As shown in Figure 6, the accuracy of the numerical simulation for nonlinear wave evolution is verified by comparing it to the physical experiment. The case of a wave period $T = 1.2$ s and a wave amplitude $a = 0.02$ m is used for verification here. Figure 6 shows the time series of the free surface elevation at $x = 9.36$ m, and it can be seen that the calculation results are in good agreement with the experimental data.

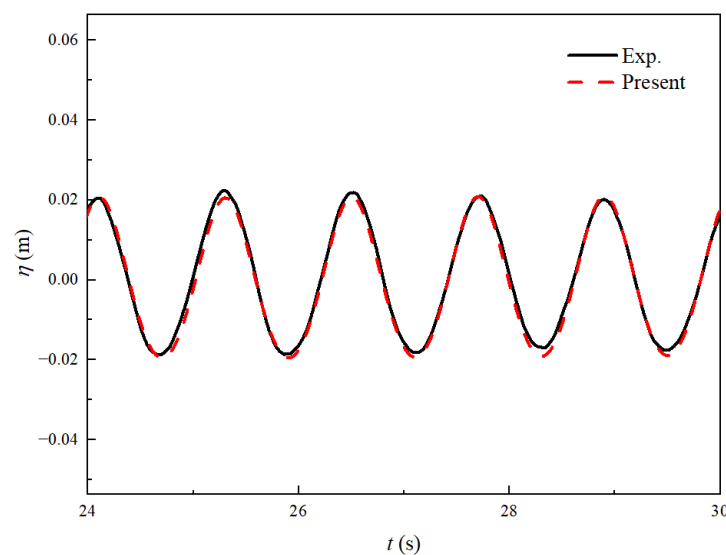


Figure 6. The time series of the free surface elevation at $x = 9.36$ m without submerged plate.

3.1.3. Numerical Model for Wave-Submerged Plate Interaction

Then, an inclined submerged plate is placed at $x = 9.36$ m for nonlinear wave-plate interactions. The structure dimensions considered in both physical experiments and the numerical simulations are: the inclined angle $\alpha = 30^\circ$, the submerged depth $d' = 0.25$ m, the plate thickness $w = 0.01$ m, and the plate length $L = 0.4$ m, see Figure 2. Again, the wave period $T = 1.2$ s and wave amplitude $a = 0.02$ m were used here for validation.

Similar to the simulations in Figures 5 and 6, a convergence analysis is firstly carried out, see Figure 7, where the time series of the free surface elevation calculated by the three different mesh sizes are shown. The background mesh (i.e., the mesh for the pure wave tank) is the same as those in Figure 5, and the mesh size on the plate surface is tested here. According to Figure 7, the medium mesh of $L/30$ is then selected for use in this work.

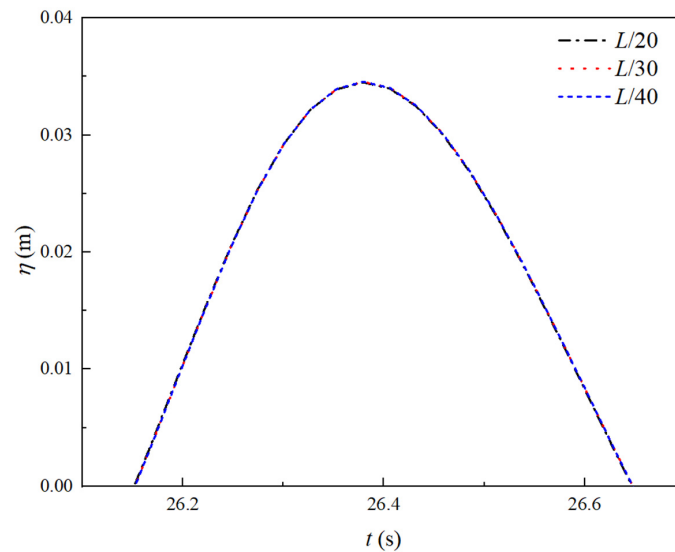


Figure 7. Time series of the free surface elevation at $x = 8\lambda$ calculated using three different mesh sizes on the submerged plate surface.

Figure 8a–c shows the comparisons between the experimental and numerical results for G_1 on the weather side, G_5 directly above the plate, and G_7 on the leeward side (see Figure 2), respectively. These confirm NWT’s ability to simulate nonlinear wave-submerged plate interactions.

3.1.4. Verification with the FEM Simulations by Nallayarasu

Nallayarasu carried out a set of numerical simulations on a submerged inclined plate of various inclination angles using a finite element method [23]. The transmission and reflection coefficients by a submerged plate at various submerged depths are calculated.

The wave and structure parameters considered were: $d/\lambda = 0.3$, $d'/d = 0.5$ and $L/d = 0.8$. The inclination angle ranged from 0° to 80° ; with a stepping of 10° .

Figure 9 shows the variation of the transmission and reflection coefficients with the inclination angle. Both numerical results by the established NWTs and in [23] are included. The incident and reflected waves in front of the structure are separated using the aforementioned four-point method. It can be seen that numerical results agree well with the results using the finite element method (FEM) in [23], confirming the capability of the NWTs in modeling both nonlinear wave evolution and their nonlinear interaction with the submerged plate of various inclination angle. The accuracy and the applicability of the four-point method are also verified. Table 1 summarizes the relative errors between the present numerical solutions and the results from [23] in terms of the transmission and reflection coefficients (as shown in Figure 9), and we find that the relative errors for all cases/inclination angles considered are less than 10%. In addition, the energy conservation relation $k_t^2 + k_r^2 \approx 1$ is satisfied.

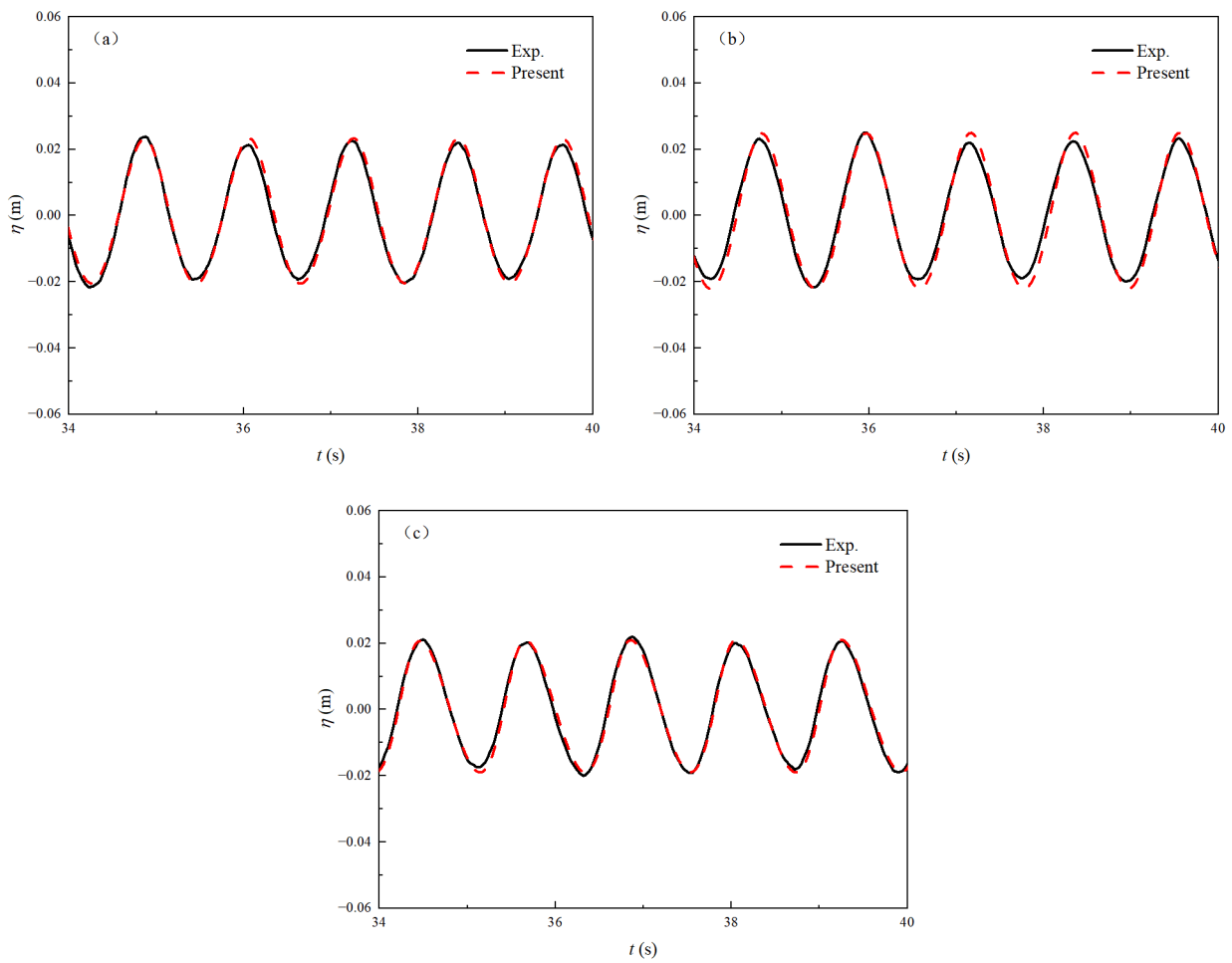


Figure 8. The time series of the free surface elevation at (a) G_1 , (b) G_5 and (c) G_7 with an inclined submerged plate in place.

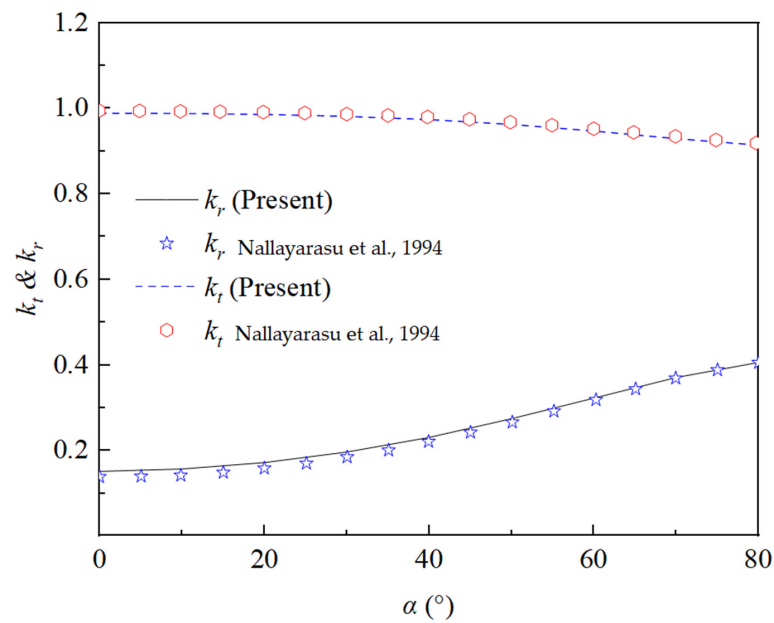


Figure 9. Variations of the transmission coefficient k_t and the reflection coefficient k_r with the inclination angle α [23].

Table 1. The relative error analysis.

α (°)	k_t [23]	k_t (Present)	Error (%)	k_r [23]	k_r (Present)	Error (%)	$k_t^2 + k_r^2$ [23]	$k_t^2 + k_r^2$ (Present)
0	0.9946	0.9890	0.5650	0.1386	0.1513	9.2169	1.0084	1.0010
10	0.9930	0.9882	0.4854	0.1441	0.1571	9.0423	1.0069	1.0012
20	0.9912	0.9858	0.5408	0.1586	0.1719	8.3333	1.0076	1.0014
30	0.9867	0.9813	0.5493	0.1849	0.1964	6.2355	1.0078	1.0015
40	0.9799	0.9739	0.6072	0.2209	0.2307	4.4360	1.0089	1.0017
50	0.9680	0.9626	0.5599	0.2662	0.2745	3.1223	1.0078	1.0019
60	0.9527	0.9471	0.5794	0.3186	0.3224	1.2054	1.0090	1.0010
70	0.9349	0.9294	0.5851	0.3693	0.3705	0.3385	1.0103	1.0011
80	0.9190	0.9142	0.5233	0.4055	0.4059	0.1036	1.0090	1.0005

3.2. Generation of Higher-Order Harmonic Free Waves

The verified model is then used to investigate the influence of the inclination angle and the incident wave amplitude on the generation of higher harmonics. Five sets of numerical experiments shown in Table 2 are considered, and the remaining parameters are the same as those in Figure 7. Case 1, Case 2 and Case 3 are designed to study the influence of the inclination angle and Cases 4–5 to investigate the influence of the wave steepness ka , which is a dimensionless parameter for describing the wave nonlinearity. The interval of the inclination angle is 10° for Cases 1–3.

Table 2. Cases setup.

Case	ka	α
Case 1	0.075	0~80°
Case 2	0.094	0~80°
Case 3	0.113	0~80°
Case 4	0.075~0.113	20°
Case 5	0.075~0.113	30°

Figure 10a,b shows the variations of the amplitude of the second-order reflected and transmitted free wave with the inclination angle, respectively. It can be seen that the amplitude of the second-order reflected free wave at the weather side increases with the inclination angle, which is similar to that of the fundamental wave shown in Figure 9. While the trend for the second-order transmitted free wave at the leeward side is different, the second-order transmitted wave now increases rather than decreases with the inclination angle. It is not surprising that the total reflection increases and transmission decreases with the inclination angle. The blocking effect of the plate is enhanced accordingly. More energy is transferred from the fundamental transmitted wave to the second-order free wave behind the plate due to the increased shallow-water effect for a larger inclination angle. Thus, the amplitude of the 2nd order free wave is increased even though the total amount of transmission is decreased.

It also can be seen from Figure 10 that a larger wave steepness ka leads to larger wave amplitudes of both the second-order reflected and transmitted free waves due to the stronger wave nonlinearity. The amount of increase is larger when the inclination angle is larger. It is interesting to see that the second-order reflected and transmitted free waves increase gradually and nearly linearly with the wave steepness ka , respectively.

The variations of the wave amplitudes of both the second-order reflected and transmitted free waves with the wave steepness ka are further investigated in Figure 11a,b, respectively. Obviously, their amplitudes increase gradually with the wave steepness ka . Moreover, it is found that they follow a quadratic relationship, although the coefficients for the reflected and transmitted waves and for each inclination angle may be different. More specially, they satisfy

$$a^r_2/a = 0.094(ka) - 0.215(ka)^2 \quad \text{for } \alpha = 20^\circ \text{ at the leeward side of the plate} \quad (19)$$

$$a^r_2/a = 0.129(ka) - 0.228(ka)^2 \quad \text{for } \alpha = 30^\circ \text{ at the leeward side of the plate} \quad (20)$$

$$a^t_2/a = -0.005 + 1.179(ka) - 1.984(ka)^2 \quad \text{for } \alpha = 20^\circ \text{ at the weather side of the plate} \quad (21)$$

$$a^t_2/a = -0.008 + 1.565(ka) - 3.254(ka)^2 \quad \text{for } \alpha = 30^\circ \text{ at the weather side of the plate} \quad (22)$$

where a^r_2/a represents the dimensionless amplitude of the second-order free wave, and ka represents the wave steepness.

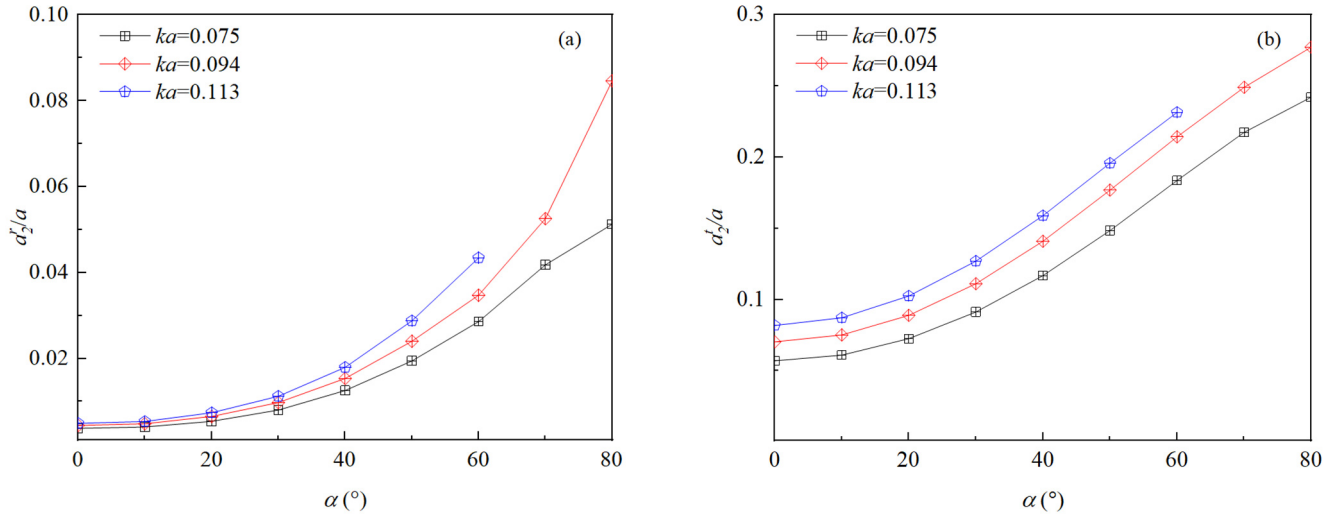


Figure 10. Variations of the amplitude of the 2nd-order reflected free wave at the weather side (a) and of the 2nd-order transmitted wave at the leeward side (b) of the plate with the inclination angle.

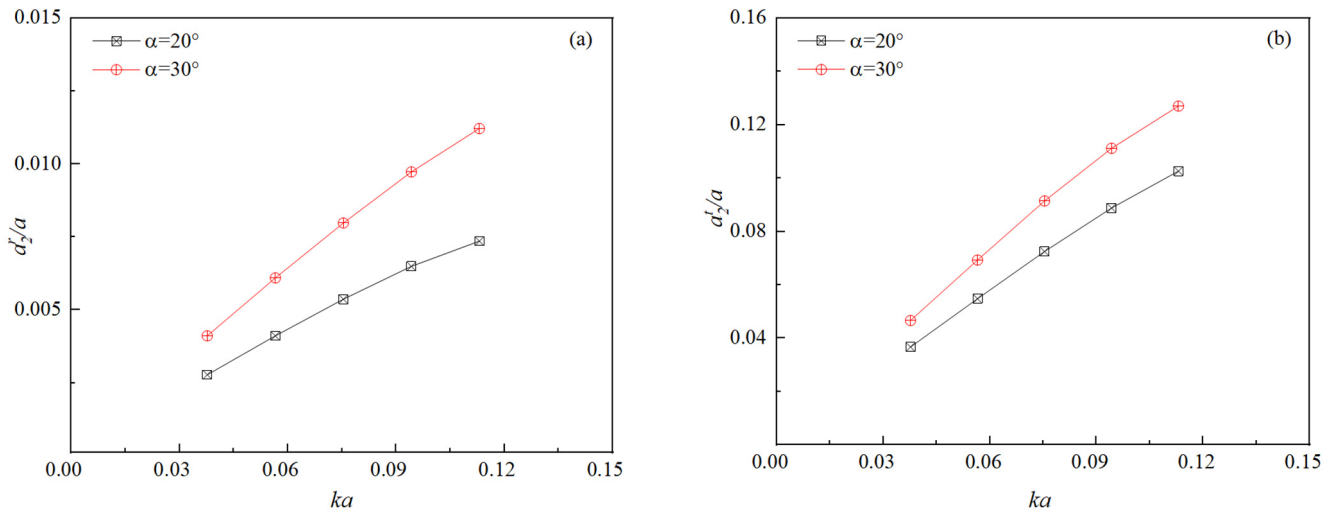


Figure 11. Variations of the amplitude of the 2nd-order reflected free wave at the weather side (a) and of the 2nd-order transmitted wave at the leeward side (b) of the plate with the wave steepness ka .

Figure 12a,b shows the spatial distribution of first-order and second-order harmonic amplitudes along the x direction, respectively. The separated harmonics can be obtained by applying the Fourier transform of Equation (10). Figure 12a shows the spatial distribution of the first-order harmonic wave amplitude, i.e., linear component. It can be seen that its amplitude tends to decrease with the inclination angle. It can be seen that in the range of working conditions considered, the larger the inclination angle of the submerged plate is, the better the wave dissipation performance is, which coincides with the information reflected in Figure 9.

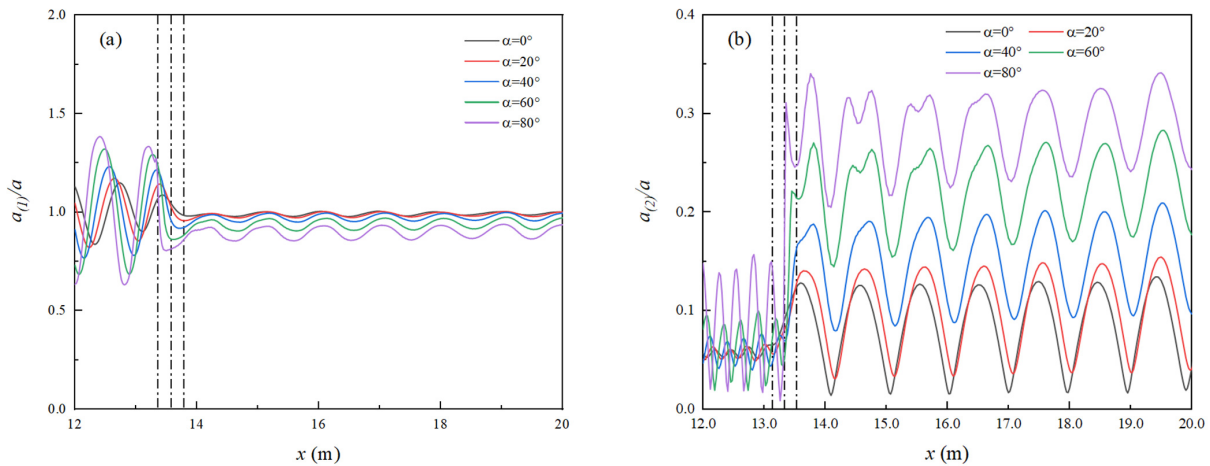


Figure 12. Spatial distribution of the first-order (a) and the second-order (b) harmonic amplitudes along x direction. The black dotted lines indicate the starting, central and the ending positions of the plate.

In contrast, the amplitude of the higher-order harmonics (Figure 12b) increases with the inclination angle, which is the same as that of the second-order free wave shown in Figure 10. Moreover, the so-called beating, i.e., periodic oscillation in space, is observed due to the same phase between the bounded and free second-order harmonic waves. In addition, a stronger beating is observed in Figure 12b. It was also found that the slope of the quadratic curve is larger for a larger inclination angle, especially for the transmitted waves, which may be due to the small wave reflections from the end of the wave flume.

Then we study the phase variation of the first-order and the second-order harmonics along the x direction in Figure 10. It can be seen that for the first-order harmonic wave (Figure 13a), the period of the phase behind the plate is slightly smaller than that in front of the plate. While for the 2nd-order harmonic wave, an obvious sub-peak in the phase curve after $x = 5$ m and before the plate is observed. This may be introduced by the wave reflection from the submerged inclined plate. Comparing Figure 13a to Figure 13b, we found that the period of the phase of the first-order harmonic wave in front of the plate was exactly twice that of the second-order harmonic wave. However, there is no obvious relationship in terms of the harmonic waves behind the plate.

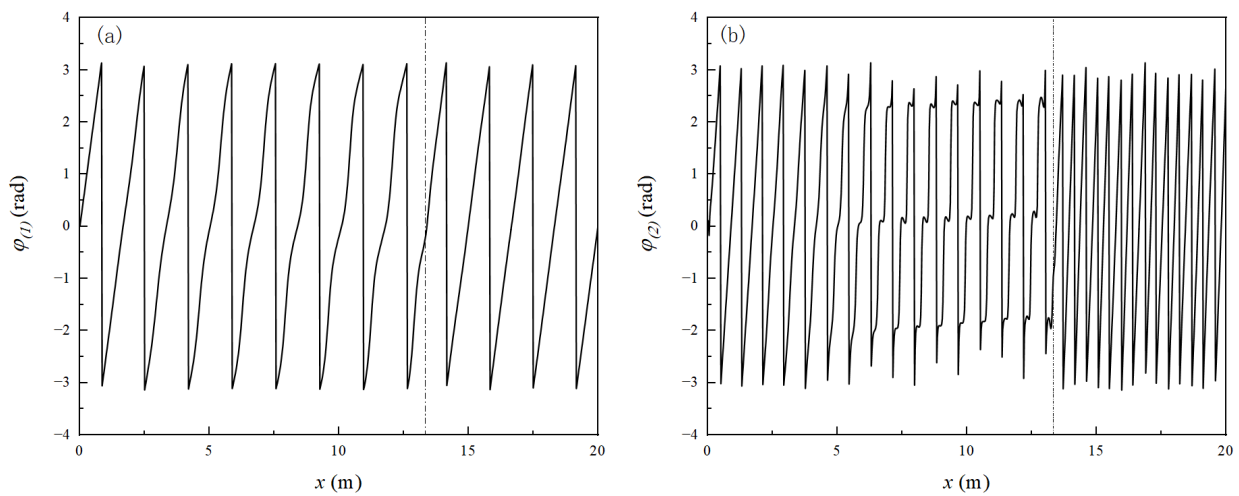


Figure 13. Spatial distribution of the phase of the first-order (a) and the second-order (b) harmonic waves along x direction. The black dotted line is the location of the plate center.

4. Conclusions

In this work, a fully nonlinear numerical wave flume is established based on the higher-order boundary element method to study the interaction between nonlinear waves and a submerged inclined plate. The bounded and free reflected and transmitted waves are separated by using the so-called four-point method. The relationships between the amplitude of the second-order free wave and the inclination angle of the submerged plate as well as the wave steepness are explored, and the phase of the higher harmonics at the weather and leeward sides of the submerged plate are analyzed. The main conclusions are as follows:

1. For a certain wave steepness ka , the amplitude of the second-order free wave at the weather and leeward sides of the submerged plate increases with the inclination angle. In addition, the larger the inclination angle is, the larger the extent of the increase is.
2. For a certain inclination angle, the amplitude of the second-order free wave in front of and behind the submerged plate increases with the wave steepness.
3. The variation of the amplitude of the second-order reflected and transmitted free waves increase gradually with the wave steepness, and a quadratic relationship is found.
4. The amplitudes of the first- and second-order harmonic wave decrease and increase with the increase of the inclination angle, respectively. The so-called beating appears due to the phase difference between the bounded and free harmonic waves.
5. The phase period of the first-order harmonic wave in front of the plate is exactly twice that of the second-order harmonic wave.

We focus on the effect of inclination angle in this work, and the performance of the submerged inclined plate will be further investigated to a wider range of wave parameters (wave periods and wave heights) and plate dimensions (plate widths and submergence depths). Thus, the results would be helpful for designing a sub-merged breakwater consisting of an inclined plate at the early design stage. In addition, the model will be extended to consider the wave-current-submerged plate interactions as the wave and current usually coexist in the real seas.

Author Contributions: Conceptualization, Z.Z. and D.N.; methodology, D.N. and L.C.; software, Y.S.; validation, Y.S.; formal analysis, Y.S. and L.C.; investigation, Y.S. and L.C.; resources, D.N.; data curation, Y.S.; writing—original draft preparation, Y.S.; writing—review and editing, L.C. and D.N.; visualization, Y.S.; supervision, D.N. and L.C.; project administration, Z.Z.; funding acquisition, D.N. and L.C.; writing-review and proof-reading, S.W. All authors have read and agreed to the published version of the manuscript.

Funding: This research was funded by the National Natural Science Foundation of China, grant number 52001053 and the Department of Science & Technology of Liaoning Province, grant number 2021-KF-16-03. The work was also funded by Liaoning Revitalization Talents Program, grant number XLYC2002033, Liaoning BaiQianWan Talents Program, grant number 2020921007, and Fundamental Research Funds for the Central Universities, grant numbers DUT21LAB116 and 1102/82232019.

Institutional Review Board Statement: Not applicable.

Informed Consent Statement: Not applicable.

Data Availability Statement: Not applicable.

Conflicts of Interest: The authors declare no conflict of interest. The funders had no role in the design of the study; in the collection, analyses, or interpretation of data; in the writing of the manuscript; or in the decision to publish the results.

References

1. Fu, D.; Zhao, X.; Wang, S.; Yan, D. Numerical study on the wave dissipating performance of a submerged heaving plate breakwater. *Ocean Eng.* **2021**, *219*, 108310. [[CrossRef](#)]
2. Liu, C.; Huang, Z.; Chen, W. A numerical study of a submerged horizontal heaving plate as a breakwater. *J. Coast. Res.* **2017**, *33*, 917–930. [[CrossRef](#)]

3. Brossard, J.; Perret, G.; Blonce, L.; Diedhiou, A. Higher harmonics induced by a submerged horizontal plate and a submerged rectangular step in a wave flume. *Coast. Eng.* **2009**, *56*, 11–22. [[CrossRef](#)]
4. He, M.; Xu, W.; Gao, X.; Ren, B. The layout of submerged horizontal plate breakwater (SHPB) with respect to the tidal-level variation. *Coast. Eng. J.* **2018**, *60*, 280–298. [[CrossRef](#)]
5. Faraci, C. Experimental Investigation of the Hydro-Morphodynamic Performances of a Geocontainer Submerged Reef. *J. Waterw. Port Coast. Ocean Eng.* **2018**, *144*, 04017045. [[CrossRef](#)]
6. Sheng, W. Wave energy conversion and hydrodynamics modelling technologies: A review. *Renew. Sustain. Energy Rev.* **2019**, *109*, 482–498. [[CrossRef](#)]
7. He, M.; Gao, X.; Xu, W.; Ren, B.; Wang, H. Potential application of submerged horizontal plate as a wave energy breakwater: A 2D study using the WCSPH method. *Ocean Eng.* **2019**, *185*, 27–46. [[CrossRef](#)]
8. Kim, J.-S.; Nam, B.W.; Park, S.; Kim, K.-H.; Shin, S.-H.; Hong, K. Numerical investigation on hydrodynamic energy conversion performance of breakwater-integrated oscillating water column-wave energy converters. *Ocean Eng.* **2022**, *253*, 111287. [[CrossRef](#)]
9. Guo, B.; Ning, D.; Wang, R.; Ding, B. Hydrodynamics of an oscillating water column WEC—Breakwater integrated system with a pitching front-wall. *Renew. Energy* **2021**, *176*, 67–80. [[CrossRef](#)]
10. Zhao, X.L.; Ning, D.Z.; Liang, D.F. Experimental investigation on hydrodynamic performance of a breakwater- integrated WEC system. *Ocean Eng.* **2019**, *171*, 25–32. [[CrossRef](#)]
11. Ji, Q.; Xu, C.; Jiao, C. Numerical investigation on the hydrodynamic performance of a vertical pile-restrained reversed L type floating breakwater integrated with WEC. *Ocean Eng.* **2021**, *238*, 109635. [[CrossRef](#)]
12. Bispo, I.B.S.; Mohapatra, S.C.; Guedes Soares, C. Numerical analysis of a moored very large floating structure composed by a set of hinged plates. *Ocean Eng.* **2022**, *253*, 110785. [[CrossRef](#)]
13. Bispo, I.; Mohapatra, S.; Soares, C.G. Numerical model of a WEC-type attachment of a moored submerged horizontal set of articulated plates. *Trends Marit. Technol. Eng.* **2022**, *2*, 335–344. [[CrossRef](#)]
14. Ursell, F. The effect of a fixed vertical barrier on surface waves in deep water. *Math. Proc. Camb. Philos. Soc.* **2008**, *43*, 374–382. [[CrossRef](#)]
15. Heins, A.E. Water waves over a channel of finite depth with a submerged plane barrier. *Can. J. Math.* **1950**, *2*, 210–222. [[CrossRef](#)]
16. Greene, T.R.; Heins, A.E. Water waves over a channel of infinite depth. *Q. Appl. Math.* **1953**, *11*, 201–214. [[CrossRef](#)]
17. Burke, J.E. Scattering of Surface Waves on an Infinitely Deep Fluid. *J. Math. Phys.* **1964**, *5*, 805–819. [[CrossRef](#)]
18. Patarapanich, M. Maximum and zero reflection from submerged plate. *J. Waterw. Port Coast. Ocean Eng.* **1984**, *110*, 171–181. [[CrossRef](#)]
19. Mohapatra, S.C.; Guedes Soares, C. Hydroelastic Response of a Flexible Submerged Porous Plate for Wave Energy Absorption. *J. Mar. Sci. Eng.* **2020**, *8*, 698. [[CrossRef](#)]
20. Grue, J. Nonlinear water waves at a submerged obstacle or bottom topography. *J. Fluid Mech.* **1992**, *244*, 455–476. [[CrossRef](#)]
21. Lin, H.-X.; Ning, D.-Z.; Zou, Q.-P.; Teng, B.; Chen, L.-F. Current effects on nonlinear wave scattering by a submerged plate. *J. Waterw. Port Coast. Ocean Eng.* **2014**, *140*, 04014016. [[CrossRef](#)]
22. Ning, D.; Chen, L.; Lin, H.; Zou, Q.; Teng, B. Interaction mechanisms among waves, currents and a submerged plate. *Appl. Ocean Res.* **2019**, *91*, 101911. [[CrossRef](#)]
23. Nallayarasu, S.; Cheong, H.F.; Shankar, N.J. Wave induced pressures and forces on a fixed submerged inclined plate. *Finite Elem. Anal. Des.* **1994**, *18*, 289–299. [[CrossRef](#)]
24. Gayen, R.; Mondal, A. Water wave interaction with two symmetric inclined permeable plates. *Ocean Eng.* **2016**, *124*, 180–191. [[CrossRef](#)]
25. Murakami, H.; Itoh, S.; Hosoi, Y.; Sawamura, Y. Wave induced flow around submerged sloping plates. In Proceedings of the 24th International Conference on Coastal Engineering, Kobe, Japan, 23–28 October 1994.
26. Rao, S.; Shirlal, K.G.; Varghese, R.V.; Govindaraja, K.R. Physical model studies on wave transmission of a submerged inclined plate breakwater. *Ocean Eng.* **2009**, *36*, 1199–1207. [[CrossRef](#)]
27. Ning, D.Z.; Zang, J.; Liu, S.X.; Eatock Taylor, R.; Teng, B.; Taylor, P.H. Free-surface evolution and wave kinematics for nonlinear uni-directional focused wave groups. *Ocean Eng.* **2009**, *36*, 1226–1243. [[CrossRef](#)]
28. Baddour, R.E.; Song, S.W. Interaction of higher-order water waves with uniform currents. *Ocean Eng.* **1990**, *17*, 551–568. [[CrossRef](#)]
29. Hunt, J.N. Direct solution of wave dispersion equation. *J. Waterw. Port Coast. Ocean Div.* **1979**, *105*, 457–459. [[CrossRef](#)]
30. Bai, W.; Eatock Taylor, R. Higher-order boundary element simulation of fully nonlinear wave radiation by oscillating vertical cylinders. *Appl. Ocean Res.* **2006**, *28*, 247–265. [[CrossRef](#)]
31. Ning, D.Z.; Teng, B. Numerical simulation of fully nonlinear irregular wave tank in three dimension. *Int. J. Numer. Methods Fluids* **2007**, *53*, 1847–1862. [[CrossRef](#)]
32. Goda, Y.; Suzuki, Y. Estimation of incident and reflected waves in random wave experiments. *Coast. Eng.* **1976**, *48*, 828–845. [[CrossRef](#)]
33. Mansard, E.; Funke, E. The measurement of incident and reflected spectra using a least squares method. In Proceedings of the 17th International Conference on Coastal Engineering, Sydney, Australia, 23–28 March 1980; ASCE Library: Reston, VA, USA, 1980; pp. 154–172. [[CrossRef](#)]
34. Mansard, E.; Sand, S.; Funke, E. *Reflection Analysis of Non-Linear Regular Waves*; Hydraul. Lab. Technol. Rep. TR-HY-011; National Research Council: Ottawa, ON, Canada, 1985; 38p.

35. Lin, C.-Y.; Huang, C.-J. Decomposition of incident and reflected higher harmonic waves using four wave gauges. *Coast. Eng.* **2004**, *51*, 395–406. [[CrossRef](#)]
36. Faraci, C.; Scandura, P.; Foti, E. Reflection of Sea Waves by Combined Caissons. *J. Waterw. Port Coast. Ocean Eng.* **2015**, *141*, 04014036. [[CrossRef](#)]
37. Ning, D.; Li, Q.; Lin, H.; Teng, B. Numerical investigation of nonlinear wave scattering by a horizontal submerged plate. *Procedia Eng.* **2015**, *116*, 237–244. [[CrossRef](#)]